AIP | Journal of Applied Physics

CdS nanofilms: Synthesis and the role of annealing on structural and optical properties

Suresh Kumar, Pankaj Sharma, and Vineet Sharma

Citation: J. Appl. Phys. **111**, 043519 (2012); doi: 10.1063/1.3688042
View online: http://dx.doi.org/10.1063/1.3688042
View Table of Contents: http://jap.aip.org/resource/1/JAPIAU/v111/i4
Published by the American Institute of Physics.

CdS nanofilms: Synthesis and the role of annealing on structural and optical properties

Suresh Kumar, Pankaj Sharma,[a] and Vineet Sharma
Department of Physics, Jaypee University of Information Technology, Waknaghat, Solan, H.P. (173234) India

(Received 16 July 2011; accepted 30 January 2012; published online 27 February 2012)

Cadmium sulfide (CdS) nanofilms have been deposited on the glass substrate using the chemical bath technique. Cadmium chloride and thiourea have been used as Cd^{2+} and S^{2-} ion sources with ammonia as a complexing agent in the presence of a nonionic surfactant. The deposited films have been annealed in air at 373 K, 473 K, 573 K, and 673 K ± 5 K temperature. The effect of the annealing on the structure, morphology, and optical properties of CdS nanofilms has been studied. CdS films have been characterized by X-ray diffraction, scanning electron microscopy, energy dispersive x-ray analysis, and UV-Vis-NIR spectrophotometer. The CdS films have been found to be nanocrystalline in nature with the zinc blende structure. The direct bandgap has been determined. Various parameters, viz. the grain size, inter-planer spacing, lattice constant, dislocation density, microstrain, surface morphology, absorption coefficient, and optical bandgap has been calculated and found to vary with annealing. The results have been explained on the basis of structural, surface, and optical changes. © *2012 American Institute of Physics*. [http://dx.doi.org/10.1063/1.3688042]

I. INTRODUCTION

The size of deposited films plays an important role and the properties of films of nano size change remarkably. Nanofilms are quasi-two dimensional structures which exhibit unusual behavior compared to their bulk counterparts. These films are strongly influenced by surface and interface effects. Nanofilms have a wide range of applications in the fields of solid state emission, solar cells, chemical sensors, piezoelectric transducers, transparent electrodes, photo-catalysts, electroluminescent devices, and ultraviolet laser diodes. The wide bandgap (1-3 eV) metal chalcogenide semiconducting films have gained various potential applications in optoelectronics, waveguides, lasers, optical sensors, photovoltaics, etc.[1] In II-IV compounds, CdS is the most promising material for detecting visible radiations.[2] The CdS films are highly favorable for heterojunction thin film solar cell applications because of their novel optical bandgap, photoconductivity, high electron affinity, and stability.[3] These films are frequently used as n-type window layers in many p-type semiconductors, such as CdTe, Cu_2S, Cu(In,Ga)Se_2, and $CuInSe_2$ based PV solar cells.[4,5] The photovoltaic solar cells fabricated using CdS film as buffer layer have been able to achieve high efficiency (10%-17%).[6–8] Films of II-VI semiconductors can be deposited using various techniques.[9–13] Chemical bath deposition (CBD) is the simplest, non-expensive, low temperature and economical way for large area deposition. The CBD is a slow deposition route which facilitates better orientation of grains with improved gain structure.

In the present paper, synthesis of CdS films of nano size have been reported using CBD and the effect of thermal annealing has been studied on the structure, morphology, and optical properties by making use of X-ray diffraction (XRD), scanning electron microscopy (SEM), energy dispersive X-ray analysis (EDAX), and UV-Vis-NIR spectrophotometer. In the reported work, the authors have grown highly uniform stoichiometric CdS nanofilms over a large area by employing the CBD method by using low molar concentration of reagents unlike using conventional high molar concentration. Grown nanofilms have been found to be homogeneous, single phase, and devoid of cracks and pinholes.

II. EXPERIMENTAL DETAILS

A. Deposition of CdS nanofilms

Nanofilms of CdS have been deposited on well cleaned glass substrates with dimensions 35 × 25 × 1 mm. The chemicals, cadmium chloride anhydrous, thiourea, ammonia solution, and triton (TX-100) [Merck, AR grade] have been used as-received without further purification. Double distilled water (Millipore, 15 MΩ-cm) has been used as a solvent. For deposition of nanofilms of CdS, aqueous solution of cadmium chloride anhydrous [$CdCl_2H_2O$: 0.02 M] has been taken in a glass beaker to which ammonia solution [NH_4OH: 25%] is added drop wise until the solution becomes clear and transparent. Thereafter, TX-100 dissolved in double distilled water is added. The solution has been vigorously stirred for 15 min to obtain a clear homogeneous solution. Finally, within 30 s an aqueous solution of thiourea [$(CSNH_2)_2$: 0.01 M] is added under vigorous stirring. A digital hot plate magnetic stirrer for constant stirring and to maintain constant bath temperature of 343 K ± 2 K has been used. The *p*H of the solution has been stabilized at 11 ± 0.1 during the deposition process. The films have been deposited for 1 h. The obtained films have been found to be pale-yellow, uniform, and with a good adherence to the substrate. The obtained films have been thermally annealed at

[a]Electronic addresses: sureshlakhanpal@gmail.com; pks_phy@yahoo.co.in; vneetsharma@gmail.com.

temperatures of 373 K, 473 K, 573 K, and 673 K ± 5 K in air for 1 h. During the chemical reaction mechanism, a large amount of gas bubbles have been formed in the bath. In order to eliminate the gas bubble formation during reaction, non-ionic surfactant TX-100 has been used. TX-100 completely eliminates the gas bubble formation, thus, leading to good quality of films.

The chemical reactions leading to the layer formation may be represented as

The cadmium n-amine complex ion decomposition

$$\left[Cd(NH_3)_n\right]^{2+} \rightleftharpoons Cd^{2+} + nNH_3, \text{ where } n = 1, 2, 3, \ldots, 6.$$

The hydrolysis of thiourea in alkaline solution with S^{2-} ions generation

$$CS(NH_2)_2 + 2OH^- \rightarrow CH_2N_2 + 2H_2O + S^{2-}.$$

The overall reaction is as follows:

$$\left[Cd(NH_3)_n\right]^{2+} + CS(NH_2)_2 + 2OH^- \rightarrow CdS_{film} + CN_2H_2 + nNH_3 + 2H_2O.$$

The deposition occurs when the ionic product of Cd^{2+} and S^{2-} ions exceeds the solubility product of CdS (7.1×10^{-28}).[14]

B. Characterization of the CdS nanofilms

The thickness of CdS films has been measured using Stylus Profilometer (AMBIOS XP-1). X-ray diffractograms ($2\theta = 20°$–$70°$) have been obtained using PANalytical's X'Pert PRO to study the structural parameters. The surface morphology of films have been studied using the scanning electron microscope (ZEISS EVO 40). Elemental composition has been checked using the energy dispersive X-ray analyzer (Bruker LN2 free X-Flash 4010 SDD Detector equipped with analytical Software QUANTAX 200). An optical study has been performed using a UV-Vis-NIR double beam spectrophotometer [Perkin-Elmer Lambda-750] in the wavelength range 300-1100 nm at room temperature (300 K).

III. RESULTS AND DISCUSSION

The thickness of the sample Z0 (as-deposited), annealed samples Z1 (373 K), Z2 (473 K), Z3 (573 K), and Z4 (673 K) has been calculated to be 40 nm, 41 nm, 38 nm, 40 nm, and 41 nm ± 0.01 nm, respectively, with an average roughness of 9 nm ± 0.01 nm using the stylus profilometer.

XRD patterns of as-deposited and annealed CdS nanofilms are shown in Fig. 1. XRD is a multipurpose, non-destructive technique which brings out detailed information about the crystallographic structure of natural and made up materials. All films show single broader XRD peaks indicating a nano-crystalline nature. The peak position of films is listed in Table I. The 2θ values for films have been assigned to the reflection (111) of cubic (zinc blende) structure.[15] The preferred (111) orientation is due to the controlled nucleation occurring in the film growth process and reflects the slow growth rate of the film deposition.[16] The sample Z0 has a peak at $2\theta = 26.94°$ with small intensity representing low crystallinity, but broader peak signify the nano-crystalline nature. Furthermore, the diffraction peaks become more sharp and intense with increasing annealing temperature and peak broadening goes on narrowing. A broader peak signifies smaller particle size but with an increase in annealing temperature, broadening decreases enhancing the particle size.

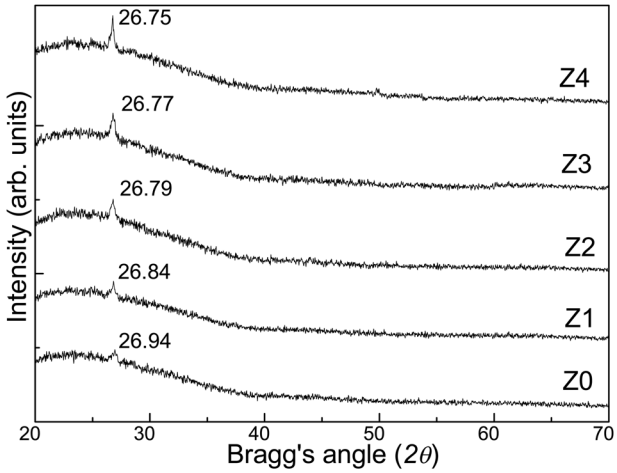

FIG. 1. XRD spectra for as-deposited film (Z0), annealed films (Z1, Z2, Z3, and Z4) CdS nanofilms.

From Fig. 1 it is clear that the full width at half maxima (FWHM) values and peak position in XRD patterns changes with annealing. The FWHM of 2θ values are related to the crystalline quality of the films. The smaller FWHM value indicates the better crystallinity of the film. For sample Z0, the FWHM value is maximum (0.5722) and with an increase in annealing temperature from 373 to 673 K, the FWHM values decreasing from 0.5425 to 0.3319. At 673 K, the film shows sharper and intense peak which represents high crystallization at this temperature with a smaller FWHM indicating a larger particle size. Figure 1 clearly specifies that the XRD peaks of reflection (111) shift toward the lower scattering angle with increase in annealing temperature. This shift may be due to an increase in grain size, an increase in lattice spacing and reduction in dislocation densities and micro-strain in the film structure (calculated later). The diffused background in XRD spectra may be either due to amorphous glass substrate or due to the presence of amorphous phase in as-deposited CdS nanofilms. As XRD peaks are small, therefore, zooming of peak position (111) has been employed to calculate corresponding $\beta_{2\theta}$ values.

TABLE I. Values of Bragg angle (2θ), grain size (D_{hkl}), d-spacing (d_{hkl}), lattice constant (a), dislocation density (ρ), microstrain (ε), and optical band gap (E_g) for CdS nanofilms for as-deposited film (Z0) and annealed films (Z1, Z2, Z3, and Z4).

Sample	2θ	D_{hkl} (nm)	d_{hkl} (Å)	a (Å)	$\rho(\times 10^{15}$ line/m^2)	ε ($\times 10^{-3}$)	E_g (eV)
Z0	26.94	14.12	3.306	5.727	5.02	2.43	2.81 ± 0.01
Z1	26.84	14.89	3.319	5.748	4.51	2.30	2.76 ± 0.01
Z2	26.79	16.96	3.325	5.759	3.48	2.02	2.49 ± 0.01
Z3	26.77	17.61	3.327	5.763	3.23	1.95	2.46 ± 0.01
Z4	26.75	24.33	3.329	5.766	1.69	1.41	2.42 ± 0.01

The grain size (D_{hkl}) for CdS films has been calculated using Scherrer's formula,[17]

$$D_{hkl} = \frac{K\lambda}{\beta_{2\theta}\cos\theta}, \quad (1)$$

where K is the shape factor and is equal to 0.89 for the zinc blende structure,[18] λ is the wavelength of X-rays (1.5406 Å for Cu-Kα), θ is the Bragg angle, and $\beta_{2\theta}$ is the angular full width at half maximum. The calculated values of grain size have been given in Table I. The sample Z4 has maximum grain size. The grain size of the CdS films increases with the increasing annealing temperature. The grain growth is 7%, 18%, 29%, and 72% for samples Z1, Z2, Z3, and Z4, respectively. With increasing annealing temperature the grain growth increases sharply. This may be due to coalescence phenomena responsible for reorganization of grains, thus, leading to densification of film taking place by filling voids and reducing strains.

The d-spacing (d_{hkl}) and lattice constant (a) for samples have been determined by using[17]

$$a = d_{hkl}\sqrt{h^2 + k^2 + l^2}, \quad (2)$$

where (hkl) are the Miller indices. The values of d_{hkl} and a are found to increase with annealing (Table I). The shift toward lower scattering angle signifies an increase in the d-spacing and lattice parameter due to grain growth from 14.12 to 24.33 nm.[19] An increase of d_{hkl} and a with increasing annealing temperature has been observed. It is clear from ASTM X-ray powder data file (10-454) that all films have lower lattice parameter in comparison to the powder sample (5.82 Å).[20] The increase of d-spacing and lattice constant due to annealing indicates that the material is inflating in films. It has also been reported by Vigil *et al.* that both d_{hkl} and a increase with increasing annealing temperature from 473 to 723 K.[20] Morales *et al.* have also reported similar variations in lattice parameters as a function of thermal annealing in $Ar + S_2$ environment for a temperature range 473-523 K.[21]

The microstrain (ε) in films has been obtained using the relation[17]

$$\varepsilon = \frac{\beta\cos\theta}{4}, \quad (3)$$

where $\beta_{2\theta}$ is the angular full width at half maximum and θ is the Bragg's angle. The dislocation density (ρ) has been evaluated from Williamson and Smallman's formula,[17]

$$\rho = \frac{n}{D_{hkl}^2} \qquad \text{lines/m}^2, \quad (4)$$

where D_{hkl} is grain size and $n = 1$ for minimum dislocation density and grain size. In CBD, deposition conditions are responsible for lattice mismatch due to impurities present in the reactant solution which may result in the development of microstrains in the films.

As the annealing temperature increases, microstrain and dislocation density of the films decreases. This may be due to dominant recrystallization which reduces lattice mismatch of the films by moving cadmium atoms from inside the grains to the grain boundaries.[22] Below 573 K annealing temperature, the grain growth is slow and particle size increases slowly. But on annealing at a temperature of 573 K and above, maximum growth of particle has been observed. This may be due to coalescence phenomenon which is responsible for reorganization of grains in the films. As a result, densification of film occurs by filling the voids and reducing the strains between grain boundaries.

Figure 2 shows the SEM micrographs (at a magnification 30 000× at the 1 μm scale) of as-deposited and annealed CdS nanofilms. Scanning electron microscopy is a convenient method for studying the microstructure of thin films and the growth of the CdS crystals on the substrate. Films are observed to be homogeneous, continuous, and exhibit complete coverage of the substrate. The surface morphology of all samples is smooth and uniform without pinholes and cracks. This may be due to the influence of TX-100. Triton acts as reducing agent in the solution, it shows low solid-water interfacial tension. The adsorption of TX-100 on the glass substrate provides better wetting property and is responsible for complete elimination of gas bubbles in the bath.[23] Small nano-sized grains are distributed uniformly in the background. These grains are very small with uniform and well defined grain boundaries.[23] The change in film surface morphology with annealing is very clear in Fig. 2. The effect of annealing is significantly slow for sample Z1 as the size of the grains (14.89 nm) increase slowly at lower annealing temperatures. Below 473 K, the agglomeration of grains is slow due to higher value of the microstrain. As annealing temperature increases (sample Z2, Z3, and Z4), the grains become larger in size and rise on the surface. SEM images reveal that the annealing enhances the tendency of coalescence of small crystallites into larger grains and shows densification of the particles. After annealing, the CdS nanofilms show denser microstructure. These results are in good agreement with those obtained from the XRD study.

The EDAX technique has been used to determine the composition of CdS nanofilms. Figure 2 shows EDAX spectrum of the as-deposited (Z0) CdS nanofilms (as reference). EDAX spectra confirm that the film contains Cd and S elements. The smaller peaks of cadmium and sulfur are also an indication of very fine particle size. EDAX spectrum also shows the signal of other elements, such as Si, Na, Ca, Mg, Al, K, and O. These elements are observed due to their presence in the glass substrate and impurities in chemicals used. On comparing the EDAX of uncoated glass substrate with the coated sample, the actual elemental composition of the CdS nanofilms has been determined and found to be stoichiometric in at %.

Figure 3 shows the transmission spectra of samples under investigation. All samples have high transmittance in visible and NIR region of solar spectrum. Relatively high transmittance of the films and sharp fall of transmission at band edge is an indication of low surface roughness and good homogeneity.[24] In general, thermal annealing tends to reduce transmittance in whole spectrum of solar light energy. Figure 3 show that transmission decreases with increase in annealing temperature. This may be due to scattering and

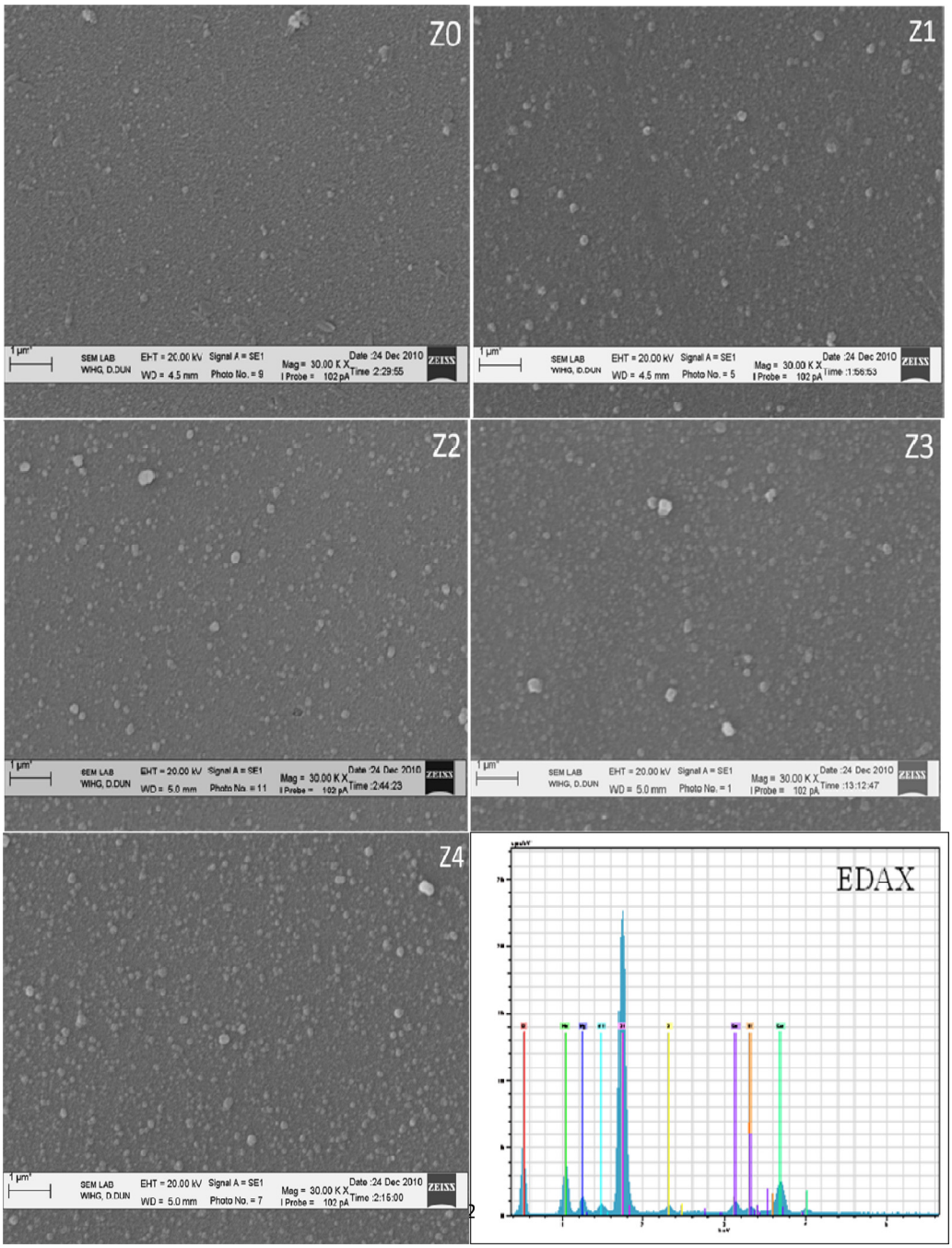

FIG. 2. (Color online) The SEM micrographs of as-deposited film (Z0) and annealed films (Z1, Z2, Z3, and Z4) and EDAX of Z0 (as reference).

absorption of light, since after annealing films become denser than as deposited film and for denser films scattering and absorption of light is higher.[24]

The optical absorption coefficient (α) due to inter-band transition near the bandgap can be calculated by[25]

$$\alpha = \frac{1}{t}\ell n\frac{1}{T}. \tag{5}$$

The value of the absorption coefficient has been determined from the spectra using (5), where T is the transmittance and t is the thickness of the film. In the higher energy region, films annealed at higher temperatures have high absorption coefficient. It has found that the value of α is minimum for as-deposited film and increases with an increase in annealing temperature. A similar trend in transmittance and absorption due to the effect of annealing has been reported in the literature.[19,26]

This may be due to the formation of larger grains as a result of annealing. These larger grains (Table I) lead to an increase in absorption. The optical absorption edge shows a shift toward longer wavelengths with annealing, i.e., redshift takes place. This redshift indicates an increase in crystallite size with increase in annealing temperature. The change in optical behavior may be due to the structural changes occurring as a result of crystallization in the films with increase in

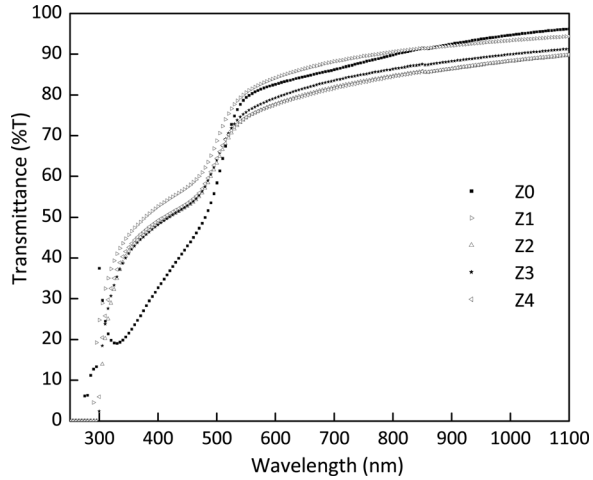

FIG. 3. Transmission spectra of as-deposited film (Z0) and annealed CdS nanofilms (Z1, Z2, Z3, and Z4).

annealing temperature. The value of the optical bandgap energy (E_g) has been determined from the absorption spectra by using Tauc's relation,[27]

$$(\alpha h\nu)^m = B(h\nu - E_g), \tag{6}$$

where α is absorption coefficient, B is a characteristic parameter independent of photon energy, $h\nu$ is incident photon energy, E_g the optical bandgap, and m is a constant which depends on the nature of the transition between the valance band and conduction band. For indirect bandgap semiconductors $m = [1/2]$ and for direct band semiconductors $m = 2$. The optical bandgap values have been estimated by extrapolating $(\alpha h\nu)^2$ versus $h\nu$. The optical bandgap values are shown in Table I. Figure 4 clearly shows that energy bandgap decreases with annealing temperature from 2.81 (Z0) to 2.42 (Z4). The decrease in E_g with increase in annealing temperature may be explained due to formation of sharp band edges because of recrystallization induced or increase in particle size with thermal annealing. The increase in annealing temperature leads to structural changes by filling the voids decreasing the defect concentration. The Urbach energy gives measurements of the defects in semiconducting materials.[28] The values of Urbach energy increases from 0.472 to 0.7924 eV for Z0 to Z4, respectively. This indicates that concentration of defects reduces with increase in annealing temperature because of increasing grain size and decrease in microstrain. This leads to dense homogeneous films with smaller bandgap. The effect of annealing is to change the film to a more ordered state with lesser amount of energy required for band to band transition. Similar variation in bandgap on annealing in air[19,20,26] and argon environment[29] has been reported by various researchers.

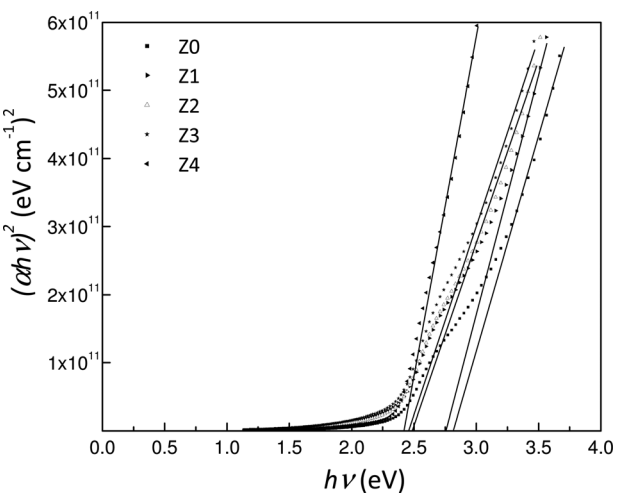

FIG. 4. Plot of $(\alpha h\nu)^2$ vs $h\nu$ for as-deposited film (Z0) and annealed CdS nanofilms (Z1, Z2, Z3, and Z4).

IV. CONCLUSION

CdS nanofilms have been deposited using the chemical bath method. The thickness of the films has been obtained to be 38 to 41 nm. The XRD study shows that films have a monocrystalline nature with (111) orientation. It has been found that grain size, d-spacing, and lattice constant increases while dislocation density and microstrain decreases with thermal annealing for a temperature range 373-673 K. SEM micrographs show that films deposited are smooth and uniform without pinhole and cracks. The optical bandgap has been found to decrease with an increase in annealing temperature. The CdS nanofilms grown using low molar concentration of chemical agents show high quality, homogeneous, and single phase stoichiometry making them suitable for use in photovoltaic and optoelectronic devices.

ACKNOWLEDGMENTS

The authors acknowledge Wadia Institute of Himalayan Geology, Dehradun for providing SEM and EDAX facilities and SAIF, P.U. Chandigarh for providing the XRD facility. The authors are grateful to Dr. Dinesh Kumar, Director, UIET, Kurukshetra University, Kurukshetra for providing the necessary facilities.

[1]M. Afzaal and P. O'Brien, J. Mater. Chem. **16**, 1597 (2006).
[2]T. Y. Wei, C. T. Huang, B. J. Hansen, Y. F. Lin, L. J. Chen, S. Y. Lu, and Z. L. Wang, Appl. Phys. Lett. **96**, 013508 (2010).
[3]C. Ferekides and J. Britt, Sol. Energy Mater. Sol. Cells **35**, 255 (1994).
[4]K. L. Chopra, P. D. Paulson, and V. Dutta, Prog. Photovolt: Res. Appl. **12**, 69 (2004).
[5]A. Romeo, D. L. Batzner, H. Zogg, C. Vignali, and A. N. Tiwari, Sol. Energy Mater. Sol. Cells **67**, 311 (2001).
[6]R. W. Birkmire and E. Eser, Annu. Rev. Mater. Sci. **27**, 625 (1997).
[7]K. Matsune, H. Oda, T. Toyama, H. Okamoto, Y. Kudriavysevand, and R. Asomoza, Sol. Energy Mater. Sol. Cells **90**, 3108 (2006).
[8]H. Kim and D. Kim, Sol. Energy Mater. Sol. Cells **67**, 297 (2001).
[9]H. Derin and K. Kantarli, Surf. Interface Anal. **41**, 61 (2009).
[10]G. Brunthaler, M. Lang, A. Forstner, C. Giftge, D. Schikora, S. Fereira, H. Sitter, and K. Lischka, J. Cryst. Growth **138**, 559 (1994).
[11]C. T. Tsai, D. S. Chuu, G. L. Chen, and S. L. Yang, J. Appl. Phys. **79**, 9105 (1996).
[12]H. Khallaf, I. O. Oladeji, G. Chai, and L. Chow, Thin Solid Films **516**, 7306 (2008).
[13]Y. J. Choi, K. J. Kim, J. B. Yoo, and D. Kim, Sol. Energy **64**, 41 (1998).
[14]G. Hodes, *Chemical Solution Deposition of Semiconductor Films* (Marcel Dekker, New York, 2002).

[15]S. Mahanty, D. Basak, F. Rueda, and M. Leon, J. Electron. Mater. **28**, 559 (1999).
[16]G. Sasikala, P. Thilakan, and C. Subramanian, Sol. Energy Mater. Sol. Cells **62**, 275 (2000).
[17]S. Prabahar and M. Dhanam, J. Cryst. Growth **285**, 41 (2005).
[18]B.D. Cullity, *Elements of X-ray Diffraction*, 2nd ed. (Addison-Wesley, Reading, MA, 1978).
[19]A. J. Haider, A. M. Mousa, and S. M. H. Al-Jawad, J. Semicond. Technol. Sci. **8**, 326 (2008).
[20]O. Vigil, O. Z. Angel, and Y. Rodriguez, Semicond. Sci. Technol. **15**, 259 (2000).
[21]R. L. Morales, M. R. Falfan, O. Z. Angel, and R. R. Bon, J. Phys. Chem. Solids **59**, 1393 (1998).
[22]C. Lei, M. Duch, I. M. Robertson, and A. Rockett, J. Appl. Phys., **108**, 114908 (2010).
[23]C. L. Perkins and F. S. Hasoon, J. Vac. Sci. Technol. A **24**, 497 (2006).
[24]J. H. Lee, W. C. Song, J. S. Yi, K. J. Yang, W. D. Han, and J. Hwang, Thin Solid Films **431–432**, 349 (2003).
[25]P. Sharma and S. C. Katyal, Mater. Lett. **61**, 4516 (2007).
[26]H. Metin and R. Esen, J. Cryst. Growth. **258**, 141 (2003).
[27]J. Tauc, *Optical Properties of Non-Crystalline Solids* (North-Holland, Amsterdam, 1972).
[28]S. F. Ahmed, M. W. Moon, C. Kim, Y. J. Jang, S. Han, J. Y. Choi, W. W. Park, and K. R. Lee, Appl. Phys. Lett. **97**, 081908 (2010).
[29]H. Metin and R. Esen, Semicond. Sci. Technol. **18**, 647 (2003).